ASTRONOMY & ASTROPHYSICS
SUPPLEMENT SERIES

Astron. Astrophys. Suppl. Ser. **126,** 325-334 (1997)

A catalogue of compact radio sources in and behind the Large Magellanic Cloud⋆

M. Marx[1], **J.M. Dickey**[1,2], **and U. Mebold**[1]

[1] Radioastronomisches Institut der Universität Bonn, Auf dem Hügel 71, D-53121 Bonn, Germany
[2] Department of Astronomy, University of Minnesota, Minneapolis, Minnesota 55455, U.S.A.

Received January 19; accepted March 10, 1997

Abstract. We present the results of a continuum snapshot survey of a $3^\circ \times 4^\circ$ region of the Large Magellanic Cloud including the area of the giant molecular cloud and the 30 Doradus nebula. The observations have been carried out with the Australia Telescope Compact Array (ATCA)[1] at 1.4 and 2.4 GHz. Most fields are complete to about 6 mJy peak flux density at 1.4 GHz and to about 3 mJy at 2.4 GHz. The positions, peak and integral flux densities of 113 compact ($< 54''$) sources detected at 1.4 GHz and of 70 sources ($< 34''$) detected at 2.4 GHz are presented. Positions are accurate to about $3''$ and peak flux densities are accurate to about 10% or better, depending on the source position relative to the pointing centers. 32 of the sources detected at 1.4 GHz are coincident with Hα objects in the catalogue of Davies et al.; these are possibly intrinsic to the LMC. However, we suppose that most are background objects, since the number vs. flux agrees with predictions of extragalactic source counts from other surveys.

Key words: Magellanic Clouds — radio continuum: galaxies — surveys — HII regions — methods: statistical

1. Introduction

The radio-continuum emission of the LMC has been investigated numerous times at several frequencies. The first catalogue of radio sources in the LMC (MC catalogue) was obtained by McGee et al. (1972a,b). They observed the LMC with the Parkes radio telescope at 5 GHz and 2.7 GHz. As a part of the whole sky survey at 0.408 GHz the LMC has been observed by Clark et al. (1976) using the Molonglo radio telescope. They detected 227 sources presented in the MC4 catalogue. Recent surveys of the LMC include the observations with Parkes at several frequencies (1.4 GHz, 2.45 GHz, 4.75 GHz and 8.55 GHz) (Filipovic et al. 1995) revealing 469 discrete sources, the PMN southern sky survey at 4.85 GHz (Wright et al. 1994) and the MOST survey at 0.843 GHz (Mills et al. 1984a,b; Ye et al., in preparation).

The Australia Telescope Compact Array (ATCA) offers the possibility of surveying compact sources in and behind the LMC with much higher spatial resolution than has been possible previously. Here we present the results of a short (12 min per field) ATCA continuum survey ("snapshot" survey) at 1.4 GHz and 2.4 GHz in the region of the giant molecular cloud and 30 Doradus.

This catalogue of compact (subarcminute) sources is useful for several purposes. Compact sources are needed to search for neutral-hydrogen 21 cm-line absorption. To study the cool ($T \lesssim 100$ K) atomic gas in the LMC an interferometer is necessary, because it acts as a spatial filter, removing the extended emission which confuses the absorption measurement. Baselines longer than about 800 m (3000 wavelengths) are needed (Dickey et al. 1994; Marx et al. in preparation), so the background sources must be smaller than about $50''$. The deepest survey of the LMC with sufficiently high angular resolution, the MOST survey ($0.75'$), is not sensitive enough to include all sources which are useful for an HI-absorption study of the LMC. A list of point sources complete to about 6 mJy peak flux density at 1.4 GHz and to about 3 mJy at 2.4 GHz is given by the present ATCA snapshot survey.

The compact radio sources in directions towards the LMC are also interesting in themselves. Most compact radio sources are background objects like quasars or Seyfert galaxies. But there are also compact objects located within the LMC. These intrinsic sources are of peculiar interest, as they might be compact HII regions (Habing & Israel 1979), young supernova remnants or planetary nebulae.

Send offprint requests to: M. Marx

⋆ Tables 3 and 4 are also available electronically at the CDS via ftp cdsarc.u-strasbg.fr (130.79.128.5) or via http://cdsweb.u-strasbg.fr/Abstract.html

[1] The Australia Telescope is funded by the Commonwealth of Australia for operation as a National Facility managed by CSIRO.

Table 1. Field centre positions and completeness levels

Field No.	R.A. [h m s] (J2000)	Dec. [° ′ ″]	C-level [mJy] 21 cm	13 cm	Field No.	R.A. [h m s] (J2000)	Dec. [° ′ ″]	C-level [mJy] 21 cm	13 cm
1D1	05 20 00.0	−67 15 00	7.5	5.5	1D5	05 20 00.0	−69 15 00	5.1	2.2
2D1	05 25 35.2	−67 15 00	5.5	4.5	2D5	05 25 35.2	−69 15 00	11.0	3.3
3D1	05 31 10.5	−67 15 00	5.5	2.0	3D5	05 31 10.5	−69 15 00	4.0	2.0
4D1	05 36 46.1	−67 15 00	6.0	6.0	4D5	05 36 46.1	−69 15 00	35.0	13.0
5D1	05 42 21.4	−67 15 00	3.0	2.0	5D5	05 42 21.4	−69 15 00	13.0	6.6
6D1	05 47 52.0	−67 15 00	2.0	2.0	6D5	05 47 52.0	−69 15 00	6.0	2.1
1D2	05 20 00.0	−67 45 00	8.0	3.0	1D6	05 20 00.0	−69 45 00	6.0	5.2
2D2	05 25 35.2	−67 45 00	5.5	3.1	2D6	05 25 35.2	−69 45 00	not complete	
3D2	05 31 10.5	−67 45 00	9.0	8.7	3D6	05 31 10.5	−69 45 00	6.0	2.5
4D2	05 36 46.1	−67 45 00	5.0	2.1	4D6	05 36 46.1	−69 45 00	7.0	6.6
5D2	05 42 21.4	−67 45 00	5.0	1.9	5D6	05 42 21.4	−69 45 00	12.0	4.1
6D2	05 47 52.0	−67 45 00	7.0	2.2	6D6	05 47 52.0	−69 45 00	4.5	2.4
1D3	05 20 00.0	−68 15 00	5.5	2.0	1D7	05 20 00.0	−70 15 00	3.0	4.6
2D3	05 25 35.2	−68 15 00	6.0	2.4	2D7	05 25 35.2	−70 15 00	4.0	3.0
3D3	05 31 10.5	−68 15 00	3.8	2.3	3D7	05 31 10.5	−70 15 00	4.5	2.4
4D3	05 36 46.1	−68 15 00	3.0	2.3	4D7	05 36 46.1	−70 15 00	4.5	3.1
5D3	05 42 21.4	−68 15 00	8.0	4.0	5D7	05 42 21.4	−70 15 00	3.0	3.0
6D3	05 47 52.0	−68 15 00	4.0	3.5	6D7	05 47 52.0	−70 15 00	5.0	3.4
1D4	05 20 00.0	−68 45 00	3.0	2.3	1D8	05 20 00.0	−70 45 00	7.0	4.8
2D4	05 25 35.2	−68 45 00	3.5	2.5	2D8	05 25 35.2	−70 45 00	14.0	7.4
3D4	05 31 10.5	−68 45 00	4.0	2.3	3D8	05 31 10.5	−70 45 00	4.0	2.7
4D4	05 36 46.1	−68 45 00	8.0	2.6	4D8	05 36 46.1	−70 45 00	4.5	2.9
5D4	05 42 21.4	−68 45 00	10.0	2.3	5D8	05 42 21.4	−70 45 00	6.0	3.9
6D4	05 47 52.0	−68 45 00	11.0	5.2	6D8	05 47 52.0	−70 45 00	7.0	3.4

A list of compact radio sources is the first step toward identifying such objects.

2. Observations and reduction

2.1. Observations

The observations were carried out with the ATCA in July 1992 using the 6D configuration including baselines between 77 m and 5878 m. The observed region extends from $5^{\rm h}18^{\rm min}$ to $5^{\rm h}50^{\rm min}$ in R.A. and $-71°$ to $-67°$ in Dec. (positions are in J2000). This area of 12 square degrees has been divided into 6×8 fields. The centre position of each of the 48 fields is given in Table 1. Three observations were taken per field with a time seperation of about 4 hours. The total integration time was 12 minutes for each field. Observations at two frequencies, 1.38 GHz and 2.378 GHz, have been carried out simultaneously. The angular resolution at 1.4 GHz is $7''$ and at 2.4 GHz it is $4''$. The primary beam has a HPW of $32'$ at 1.4 GHz and $22'$ at 2.4 GHz. The bandwidth of 128 MHz at each frequency has been separated into 32 spectral channels. The primary flux and bandpass calibrator was $1934-638$ (16.2 Jy at 1.4 GHz and 13 Jy at 2.4 GHz), the secondary (phase and gain) calibrators were $0407-658$ and $0252-712$. For data reduction the Astronomical Image Processing System (AIPS) in the special ATCA version was used.

2.2. The maps

The images were made using the AIPS routine MX, which combines the Fourier Transform imaging with the deconvolution of the synthesized beam. The deconvolution process uses the clean algorithm of Clark (1980) with 500 iterations. We chose the inner 18 channels of the frequency band to compute the images using the technique of multi-frequency synthesis.

The sparse uv-coverage of snapshot observations makes imaging difficult due to poor dynamic range in the maps. Extended emission is poorly sampled and cannot be adequately cleaned. We have tested several ways of selecting the data for mapping. Best results were obtained by restricting the data to baselines longer than 3 $k\lambda$ to exclude the poorly sampled extended emission. In the region around 30 Doradus only baselines above 6 $k\lambda$ are useful. We taper the uv data with a Gaussian weighting function with half width to 30% level of 15 $k\lambda$ at 1.4 GHz and 30 $k\lambda$ at 2.4 GHz. This gives synthesized beamwidths of about $10''$ at 1.4 GHz and $6''$ at 2.4 GHz (see Table 2). The shape of the synthesized beam depends on the declination. The beam has a circular shape only for fields with declination between $-69.25°$ and $-68.25°$. For higher and lower declination, the shape of the synthesized beam is more and more elongated, in the extreme case (fields at $-67.25°$) it is about $24'' \times 8''$ at 1.4 GHz. The maps are $49' \times 49'$ at 1.4 GHz and overlap slightly. At 2.4 GHz the map size is $31' \times 31'$. The maps have an rms noise level between 0.4 mJy and 1 mJy at 1.4 GHz and between 0.2 mJy and

0.6 mJy at 2.4 GHz. The theoretical rms values are 0.17 mJy at 1.4 GHz and 0.23 mJy at 2.4 GHz based on receiver noise alone. The excess is due to sidelobes from confusing sources aggravated by our limited dynamic range.

Table 2. Imaging parameters

	21 cm	13 cm
image size	1024×1024 pixels 49′×49′	1024×1024 pixels 31′×31′
cellsize	2.9″	1.8″
*uv*min (minimum spacing)	$3k\lambda$ | $6k\lambda$	$2k\lambda$ | $3k\lambda$
source size	< 54″ | < 34″	< 73″ | < 34″
number of CLEAN iterations	500	500
CLEAN loop gain	0.1	0.1
uv-taper (30% level)	$15k\lambda$ | -	$30k\lambda$
HPW of synthesized beam	≈ 10″ | ≈ 7″	≈ 6″
HPW of primary beam	32′	22′

To correct the images for primary beam attenuation the program PBCOR was used with the standard AT primary beam shape. We tested this by comparing the peak flux densities of sources detected separately in different overlapping fields. We find that the ratio of the flux densities of the same source in two fields is independent of the difference of its distances from the pointing centres. Only for some very weak sources with a large distance d (above 20′) from the field centre does this ratio differ much from one, indicating a higher uncertainty of the primary beam correction for $(d \cdot \nu)^2 > 780$.

A mosaic of the 48 final images is shown in the first figure. 3×4 fields of $49' \times 49'$ each have been combined with the AIPS routine LTESS which takes the primary beam attenuation into account. The resultant four mosaicing fields have then been combined with the task COMB, averaging the overlapping areas. The image shown is smoothed to about 1′ resolution.

2.3. Source finding

Very brief observations in the snapshot mode are ideal to study sources which are bright and compact, but the high sidelobe levels of beams synthesized from snapshots exacerbate the problems created by confusing sources. Some sidelobes cannot be completely eliminated in our cleaning process. The fields near 30 Dor are particularly compromised. Due to such sidelobe structure, the minimum detectable source flux is raised. We determined three criteria to decide which objects are real:

- The source must have signal exceeding 5 times the rms noise of the field, and
- the source must be stronger than any remaining sidelobe structure in the field, and
- the source has to be stronger than the absolute flux density value of the largest negative peak in the field.

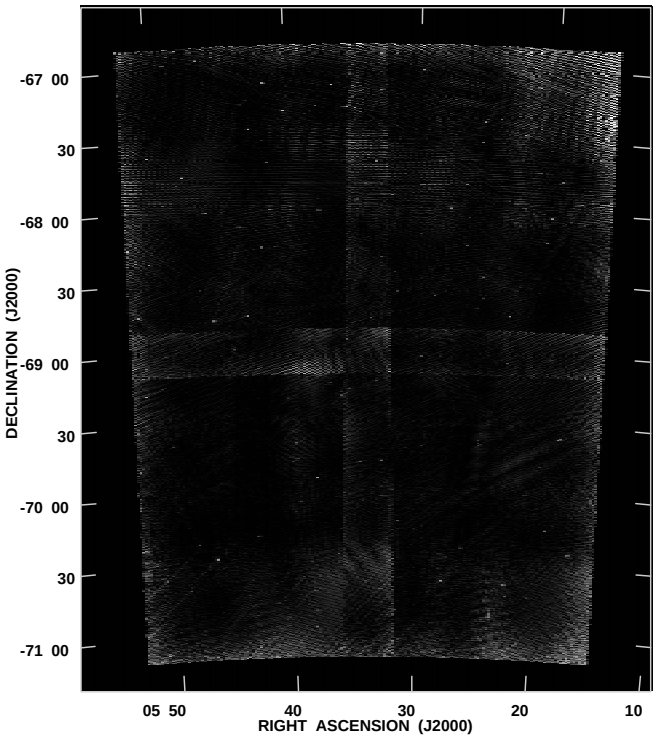

Fig. 1. Mosaic of all 48 images at 1.4 GHz. The cross feature is the overlapping area of the four combined LTESS-fields. Unreal structures with high intensity can be seen in the area of 30 Dor (05h38m40s, −69°06′09″). At the top right corner strong sidelobes are produced by a high intensity source outside the snapshot field

We used the highest of these values to determine the completeness level, C, above which the sources in the field are accepted as real. These completeness levels are listed in Table 1 uncorrected for primary beam attenuation. Most fields are complete to about 6 mJy peak flux density at 1.4 GHz and to about 3 mJy at 2.4 GHz. In field 2D6 confusion by the bright extended emission of SNR $0525-696$ makes source finding for this area impossible.

3. The source list

The positions, peak flux densities, S_p, and integrated flux densities, S_i, of the sources were determined using the AIPS routine IMFIT. The integrated flux density of a source is given by

$$S_\mathrm{i} = S_\mathrm{p} \cdot \frac{\Theta_{S\mathrm{max}} \cdot \Theta_{S\mathrm{min}}}{\Theta_{B\mathrm{max}} \cdot \Theta_{B\mathrm{min}}}$$

where $\Theta_{S\mathrm{max}}$ and $\Theta_{S\mathrm{min}}$ are the major and minor axis of the source response as fitted by a Gaussian to the map and $\Theta_{B\mathrm{max}}$ and $\Theta_{B\mathrm{min}}$ are the gaussian major and minor axis of the synthesized beam. The peak flux densities are much better determined than the integrated flux densities, because of the missing short spacings on the *uv* plane.

Table 3 lists all sources found in the survey at 1.4 GHz that fulfill the criteria described in Sect. 2.3. A sample of 113 sources is found. The source name is given in the first column. It is derived from the standard IAU system of source nomenclature (Lortet et al. 1994), namely MDM NNN (e.g. MDM 114). The letters "NNN" indicate the sequence number within the catalogue. The position of the source is listed in the next two columns. If a source has been detected in two different fields, we use the one with the closer field centre. The integral and peak flux densities are given in Cols. 4 and 5. Both of these values have been corrected for the primary beam attenuation. Columns 6 and 7 show the spacings used and the value of the tapering when imaging the data with MX. Column 8 gives the field in which the source is detected.

The maps at 2.4 GHz show a better quality than the data at 1.4 GHz. This is due to the smaller amplitude of the extended emission at the shorter wavelength. 70 point sources have been detected at 2.4 GHz; these are listed in Table 4. Source MDM 6 has not been detected at 1.4 GHz due to the less sensitivity at this frequency. The source positions at 1.4 GHz and 2.4 GHz agree very well. The position difference is mainly below 2″ and independent of the flux density of the source. For 69 sources the spectral index α, with $S_{\rm p}(\nu) \sim \nu^{\alpha}$, between 1.4 and 2.4 GHz has been estimated using the peak flux density $S_{\rm p}$. The values are listed in Col. 9. The mean spectral index for all 69 sources is $< \alpha >= -0.72 \pm 0.09$.

3.1. Missing flux density

After filtering out the extended structures, only compact objects and the cores of extended sources appear in the final images. Excluding baselines below 3 $k\lambda$ the survey is only sensitive to structures smaller than about 54″ at 1.4 GHz and 34″ at 2.4 GHz. Assuming a distance of 50 kpc for the LMC (Westerlund 1992), these values correspond to sizes smaller than 13 pc (1.4 GHz) and 8 pc (2.4 GHz). To illustrate this effect for several of our snapshot fields we added artificial 100 mJy sources of different sizes to the *uv*-data using the task UVSUB and then processed the data with MX in the same way that we had processed the field before. After mapping and cleaning the field with MX, flux is lost for the artificial source depending on its size. Figure 2 shows the distribution of the integral flux densities for artificial sources of different angular sizes. For a diameter of about 3″, we lose 10% of the flux. This loss of flux depends on the *uv*-coverage of the field. For fields where only baselines above 6 $k\lambda$ have been used because of very extended emission, much more flux is lost. If a 100 mJy source with an angular size of 3″ is added into field 5D6, the missing flux is on the order of 19%. For angular sizes above 10″, the flux drops off quite sharply. This implies that the flux densities of the snapshot sources are lower limits in the case of resolved sources.

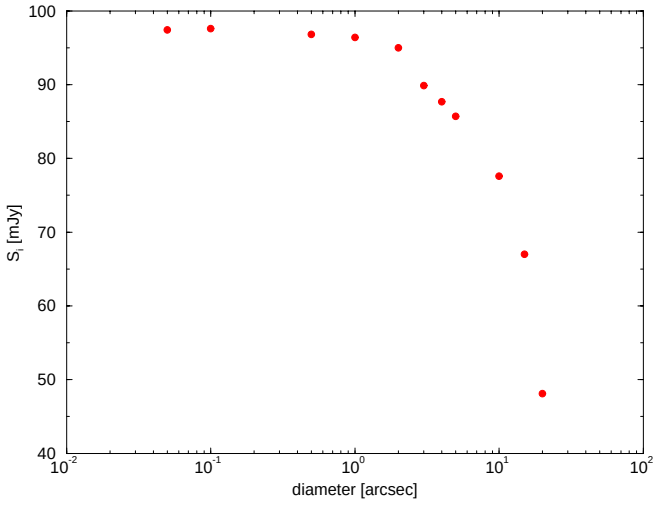

Fig. 2. Integrated flux densities for simulated 100 mJy sources of several sizes

4. Identifications

4.1. Comparison with radio observations

We compared our data with several single dish surveys of the LMC, the Molonglo observations at 408 MHz (Clarke et al. 1976) and the Parkes observations at 5 GHz (McGee et al. 1972a) and 4.75 GHz (Filipovic et al. 1995).

We identify sources of the ATCA catalogue with objects listed in the Molonglo Radio Source Catalogue 4, if the difference in position is smaller than the HPBW of the Molonglo telescope (2.′6). Nearly all sources above 50 mJy can be identified with an MC4 object (see Table 3 Col. 9). To compare the peak flux densities of both surveys, we estimated the corresponding flux density of the MC4 source at 1.4 GHz by using our spectral indices between 1.4 and 2.4 GHz (Table 4 Col. 9). There are 21 usable objects for this comparison. Most of the estimated flux densities show a much higher value compared with the measured fluxes of the ATCA sources. This discrepancy may be accounted for solely by flux loss in the Compact Array observations of extended sources as compared with the filled aperture telescope. Furthermore many compact extragalactic objects are known to be variable. However, there may also be a component of this discrepancy arising from bias in the quoted spectral indices because of the different amount of the flux loss at 1.4 and 2.4 GHz. Only a few sources show similar flux densities in both surveys. These objects (MDM 1, MDM 64, MDM 84, MDM 90, MDM 100) seem to be point sources. Due to the high resolution of the ATCA, the strong source MC4$(0524-708)$ was separated into two components.

There are only 10 sources which can be identified with objects found by McGee et al. (1972a) at 6 cm (Table 3 Col. 9), if we demand that the position difference from the ATCA object to the one of the MC-catalogue is smaller

Table 3. The source list at 1.4 GHz

Source name	R.A. (J2000) [h m s]	Dec. (J2000) [° ′ ″]	S_i [mJy]	S_p [mJy]	uvr [$k\lambda$]	uvt [$k\lambda$]	field	Identifications
MDM 1	05 17 15.95	−70 23 58.9	80	70	>3	15	1D7	MC4(0517–704), LMC B0517–7026
MDM 2	05 18 02.58	−67 55 42.3	52	36	>3	15	1D2	MC4(0518–679), LMC B0518–6759, DEM129
MDM 3	05 18 32.74	−69 35 22.8	326	288	>5	15	1D6	MC4(0518–696A), LMC B0519–6941
MDM 4	05 18 50.08	−69 09 33.6	22	23	>3	15	1D5	MC4(0519–691), LMC B0519–6916, DEM132b
MDM 5	05 18 55.39	−69 09 00.9	6	7	>3	15	1D5	MC4(0519–691), DEM132b
MDM 7	05 19 16.42	−70 14 16.1	19	19	>3	15	1D7	
MDM 8	05 19 25.72	−67 47 02.1	15	17	>3	15	1D2	
MDM 9	05 20 07.00	−68 02 24.4	64	32	>5	15	1D3	MC4(0520–680), LMC B0520–6804
MDM 10	05 20 19.27	−68 12 43.1	14	13	>5	15	1D3	
MDM 11	05 20 26.09	−70 42 51.5	8	9	>3	15	1D8	
MDM 12	05 21 05.24	−69 59 41.2	111	104	>5	15	1D6	MC4(0521–700), LMC B0521–7002
MDM 13	05 21 08.56	−67 43 31.0	30	28	>3	15	1D2	DEM151
MDM 14	05 21 18.09	−71 02 20.1	28	24	>3	15	1D8	
MDM 15	05 21 27.58	−67 07 24.1	36	35	>3	15	1D1	LMC B0521–6710
MDM 16	05 21 45.09	−70 20 48.8	5	5	>3	15	1D7	
MDM 17	05 22 17.40	−67 27 40.4	36	27	>3	15	1D1	
MDM 18	05 22 29.52	−70 37 56.8	148	135	>3	15	1D8	MC4(0523–706), LMC B0523–7040
MDM 19	05 22 56.13	−69 04 08.5	16	19	>5	15	2D5	DEM177
MDM 20	05 22 58.87	−68 44 29.3	23	22	>3	15	2D4	
MDM 21	05 23 40.94	−70 50 20.7	225	210	>3	15	2D8	MC4(0524–708), MC37, LMC B0524–7053
MDM 22	05 23 40.97	−70 51 22.3	245	220	>3	15	2D8	MC4(0524–708), MC37, LMC B0524–7053
MDM 23	05 25 05.71	−68 28 18.5	13	9	>3	15	2D3	LMC B0525–6831, DEM180
MDM 24	05 25 05.74	−68 37 00.9	9	9	>3	15	2D4	
MDM 25	05 25 17.22	−67 22 47.4	62	58	>3	15	2D1	DEM192
MDM 26	05 25 29.95	−67 31 30.5	14	10	>3	15	2D1	LMC B0526–6731, DEM192
MDM 27	05 25 33.69	−68 41 21.2	8	10	>3	15	2D4	
MDM 28	05 26 11.85	−70 22 46.8	14	14	>3	15	2D7	
MDM 29	05 26 24.43	−68 15 11.2	43	26	>3	15	2D3	DEM203
MDM 30	05 26 35.48	−67 49 09.3	95	89	>3	15	2D2	LMC B0526–6751
MDM 31	05 27 45.92	−67 59 27.1	35	37	>3	15	2D2	
MDM 32	05 27 49.22	−70 36 44.0	54	50	>3	15	2D8	MC4(0528–706), LMC B0528–7038 , DEM208
MDM 33	05 27 54.56	−69 11 40.7	15	13	>5	15	2D5	LMC B0528–6914, DEM210
MDM 34	05 28 00.03	−70 25 41.5	22	20	>3	15	3D7	
MDM 35	05 28 47.68	−68 36 23.1	22	21	>3	15	3D4	
MDM 36	05 29 47.89	−69 02 11.7	15	14	>3	15	3D5	
MDM 37	05 29 50.59	−67 01 14.7	14	11	>3	15	3D1	LMC B0529–6702, DEM214
MDM 38	05 29 51.64	−67 49 34.5	188	150	>3	15	3D2	MC4(0529–678), LMC B0529–6752
MDM 39	05 29 51.83	−68 10 18.4	6	6	>3	15	3D3	LMC B0530–6814
MDM 40	05 31 22.47	−70 11 54.6	11	12	>3	15	3D7	LMC B0531–7010
MDM 41	05 31 42.57	−68 34 53.9	7	8	>3	15	3D4	LMC B0532–6833
MDM 42	05 31 43.94	−70 49 25.8	18	18	>3	15	3D8	DEM221
MDM 43	05 31 54.71	−68 26 39.0	6	7	>3	15	3D3	LMC B0532–6833
MDM 44	05 32 07.16	−67 54 14.2	34	34	>3	15	3D2	
MDM 45	05 32 09.65	−68 43 08.1	11	11	>3	15	3D4	MC55, LMC B0532–6841, DEM226
MDM 46	05 32 11.06	−68 30 24.4	9	9	>3	15	3D3	MC56, LMC B0532–6833
MDM 47	05 32 16.50	−70 23 57.3	10	10	>3	15	3D7	
MDM 48	05 32 44.99	−70 01 28.5	75	71	>3	15	3D7	LMC B0533–7001
MDM 49	05 32 48.24	−68 23 59.3	9	9	>3	15	3D3	
MDM 50	05 32 50.32	−68 20 12.6	11	12	>3	15	3D3	
MDM 51	05 32 52.80	−69 46 22.5	33	30	>3	15	3D6	DEM246
MDM 52	05 32 53.24	−67 09 44.6	28	22	>3	15	3D1	
MDM 53	05 32 54.21	−70 40 28.4	16	15	>3	15	3D8	
MDM 54	05 33 15.32	−69 12 46.8	9	8	>3	15	3D5	DEM232
MDM 55	05 33 18.70	−67 40 00.2	29	31	>3	15	3D2	LMC B0532–6743, DEM231
MDM 56	05 33 42.44	−68 46 03.3	50	32	>3	15	3D4	LMC B0534–6847, DEM233
MDM 57	05 34 08.28	−70 37 17.4	9	11	>3	15	4D8	
MDM 58	05 34 48.37	−67 56 00.1	46	39	>3	15	4D2	MC4(0534–679)
MDM 59	05 35 24.70	−67 35 09.6	23	11	>3	15	4D2	MC4(0535–676A), MC64, LMC B0535–6736, DEM241
MDM 60	05 35 26.51	−67 17 04.5	67	56	>3	15	4D1	MC4(0535–673), LMC B0535–6718
MDM 61	05 35 37.48	−68 55 08.0	63	60	>6	0	4D4	LMC B0535–6857
MDM 62	05 36 05.06	−69 18 45.9	78	84	>6	0	4D5	DEM263
MDM 63	05 36 23.89	−70 25 43.0	9	11	>3	15	4D7	
MDM 64	05 36 36.42	−67 07 36.1	65	62	>3	15	4D1	MC4(0536–671), DEM257
MDM 65	05 36 57.17	−69 13 29.0	174	149	>6	0	4D5	MC4(0537–692A), LMC B0538–6911, DEM263
MDM 66	05 37 36.93	−68 00 34.3	35	33	>3	15	4D3	DEM268
MDM 67	05 37 56.50	−70 35 14.8	9	11	>3	15	4D8	
MDM 68	05 38 04.78	−69 53 37.5	69	62	>6	0	4D6	LMC B0538–6956
MDM 69	05 38 09.01	−70 49 32.1	10	11	>3	15	4D8	
MDM 70	05 38 16.15	−70 56 36.4	21	20	>3	15	4D8	
MDM 71	05 38 21.43	−70 41 09.3	37	22	>3	15	5D8	LMC B0538–7042, DEM265
MDM 72	05 38 44.46	−69 04 39.2	75	56	>6	0	5D5	MC4(0539–691), MC74, LMC B0539–6907, DEM263
MDM 73	05 39 29.92	−70 03 28.9	24	22	>3	15	4D7	

Table 3. continued

Source name	R.A. (J2000) [h m s]	Dec. (J2000) [° ′ ″]	S_i [mJy]	S_p [mJy]	uvr [$k\lambda$]	uvt [$k\lambda$]	field	Identifications
MDM 74	05 39 37.56	−69 45 27.1	50	41	>6	0	5D6	MC77, LMC B0540–6946, DEM271
MDM 75	05 39 45.82	−69 38 38.8	33	31	>6	0	5D6	MC4(0540–696B), MC76, DEM284
MDM 76	05 39 54.90	−70 07 45.8	12	12	>3	15	4D7	
MDM 77	05 40 02.05	−69 06 19.8	24	27	>6	0	5D5	DEM263
MDM 78	05 40 04.65	−69 44 39.6	23	21	>6	0	5D6	MC4(0540–697A), MC77, LMC B0540–6946, DEM271
MDM 79	05 40 10.39	−67 18 14.8	75	70	>3	15	5D1	LMC B0540–6719
MDM 80	05 40 11.43	−69 19 55.5	40	35	>6	0	5D5	MC4(0540–693), MC78, LMC B0540–6921, DEM269
MDM 81	05 41 16.68	−67 59 55.5	21	16	>3	15	5D2	MC4(0541–680), LMC B0541–6801
MDM 82	05 41 27.23	−67 39 52.1	44	34	>3	15	5D2	
MDM 83	05 41 31.58	−70 46 29.4	20	19	>3	15	5D8	
MDM 84	05 41 33.03	−67 06 16.6	69	62	>3	15	5D1	MC4(0541–671), LMC B0541–6707
MDM 85	05 41 59.09	−68 15 43.4	30	31	>3	15	5D3	
MDM 86	05 42 44.53	−67 25 54.4	16	14	>3	15	5D1	LMC B0543–6730
MDM 87	05 42 56.33	−70 17 36.4	12	11	>5	15	5D7	
MDM 88	05 43 06.72	−71 04 05.7	58	43	>3	15	5D8	MC4(0543–710), LMC B0543–7105
MDM 89	05 43 14.49	−68 44 36.1	74	70	>3	15	5D4	
MDM 90	05 43 15.29	−68 06 53.9	128	109	>3	15	5D3	MC4(0543–681), LMC B0543–6808
MDM 91	05 43 17.17	−67 15 09.8	7	7	>3	15	5D1	
MDM 92	05 43 56.08	−68 17 32.4	13	12	>3	15	5D3	
MDM 93	05 45 04.54	−69 39 29.7	18	14	>5	0	6D6	DEM310
MDM 94	05 45 27.65	−69 46 24.4	9	7	>5	0	6D6	LMC B0545–6947, DEM311
MDM 95	05 45 50.52	−68 45 57.8	62	53	>3	15	6D4	MC4(0546–687)
MDM 96	05 46 12.16	−68 00 15.9	21	21	>3	15	6D3	LMC B0546–6802
MDM 97	05 46 23.49	−66 55 48.2	16	13	>3	15	6D1	
MDM 98	05 46 29.15	−70 26 40.7	83	50	>5	15	6D7	MC4(0547–704)
MDM 99	05 46 52.85	−68 32 48.7	13	12	>3	15	6D3	
MDM 100	05 47 45.37	−67 45 07.1	90	83	>3	15	6D2	MC4(0547–677), LMC B0547–6746
MDM 101	05 47 50.31	−67 28 02.5	6	6	>3	15	6D1	LMC B0547–6729
MDM 102	05 47 51.41	−69 45 43.5	7	8	>5	0	6D6	LMC B0547–6942
MDM 103	05 47 57.70	−70 20 16.1	12	12	>5	15	6D7	LMC B0548–7025
MDM 104	05 48 45.46	−66 57 26.7	13	8	>3	15	6D1	
MDM 105	05 48 55.14	−70 39 26.7	21	21	>3	15	6D8	LMC B0549–7037
MDM 106	05 49 39.70	−69 38 23.6	14	14	>5	0	6D6	
MDM 107	05 50 15.89	−67 36 03.5	24	21	>3	15	6D2	
MDM 108	05 50 32.90	−68 20 55.5	48	34	>3	15	6D3	MC4(0550–683), LMC B0550–6823
MDM 109	05 50 48.97	−70 34 34.7	47	28	>3	15	6D8	
MDM 110	05 51 30.31	−69 16 32.8	91	79	>3	15	6D5	MC4(0551–692), LMC B0551–6917
MDM 111	05 51 39.49	−68 43 17.3	30	30	>3	15	6D4	MC4(0552–687), LMC B0552–6843
MDM 112	05 52 05.81	−68 14 41.9	178	153	>3	15	6D3	MC4(0552–682), LMC B0552–6815
MDM 113	05 52 27.83	−69 48 02.9	75	45	>5	0	6D6	MC4(0552–698), LMC B0552–6948
MDM 114	05 52 28.46	−70 21 37.0	56	44	>5	15	6D7	MC4(0552–703), LMC B0552–7022

than the HPBW of the Parkes telescope, which is about 4′ at 6 cm. The flux densities of all sources observed with the single dish telescope are much higher than those of the compact ATCA sources.

We identified a compact source in the snapshot field of 3°×4° with an object observed with Parkes at 4.75 GHz (Filipovic et al. 1995), if the difference in position is smaller than the HPBW of 4.′8 (Table 3 Col. 9 abbreviation LMC). For all 53 identified sources the flux density of the Parkes object is higher than the value of the ATCA source at 1.4 GHz. There is also a large position difference for most objects.

The poor correspondance between compact sources detected with the ATCA and the Parkes sources is common also in galactic plane surveys (Garwood et al. 1988), and arises from the fact that most of the continuum flux from a galaxy disk comes from structures much larger than a few parsecs, which is our effective resolution at the distance of the LMC.

From the comparison of our snapshot sources with radio objects from single dish observations, we conclude that most of our discrete objects are compact cores of extended sources or background objects.

4.2. Identification with Hα emitting objects

Comparison of the radio point source positions with Hα emitting objects helps us to find sources intrinsic to the LMC. Figure 3 shows the distribution of the compact radio sources on the Hα map of Kennicutt et al. (1995).

A compact radio source is regarded as being identified with an Hα object of the Davies-Elliot-Meaburn catalogue (DEM), if the radio source lies within the extent of the DEM object. We find 32 radio point sources associated with an Hα emitting object. These might be compact HII regions or young SNRs. Such objects can show high brightness knots embedded in the extended DEM object. Hα observations at

Table 4. The source list at 2.4 GHz

Source name	R.A. (J2000) [h m s]	Dec. (J2000) [° ′ ″]	S_i [mJy]	S_p [mJy]	uvr [$k\lambda$]	uvt [$k\lambda$]	field	α
MDM 1	05 17 16.07	−70 23 59.0	61	49	>2	30	1D7	−0.67
MDM 2	05 18 02.61	−67 55 43.3	19	16	>3	30	1D2	−1.48
MDM 3	05 18 32.72	−69 35 22.5	259	219	>3	30	1D6	−0.50
MDM 4	05 18 50.03	−69 09 32.0	6	6	>3	30	1D5	−2.55
MDM 5	05 18 55.25	−69 09 00.7	5	5	>3	30	1D5	−0.57
MDM 6	05 19 10.74	−68 15 44.4	6	6	>3	30	1D3	
MDM 7	05 19 16.38	−70 14 16.5	29	20	>2	30	1D7	+0.05
MDM 8	05 19 25.77	−67 47 01.6	11	11	>3	30	1D2	−0.79
MDM 9	05 20 07.74	−68 02 25.0	24	20	>3	30	1D3	−0.87
MDM 10	05 20 19.04	−68 12 42.7	6	5	>3	30	1D3	−1.69
MDM 11	05 20 25.85	−70 42 52.5	7	8	>3	30	1D8	−0.28
MDM 12	05 21 05.24	−69 59 41.2	91	92	>3	30	1D6	−0.22
MDM 13	05 21 08.61	−67 43 31.4	18	14	>3	30	1D2	−1.27
MDM 15	05 21 27.67	−67 07 24.3	33	30	>3	30	1D1	−0.30
MDM 18	05 22 29.55	−70 37 56.6	68	68	>3	30	1D8	−1.28
MDM 21	05 23 40.86	−70 50 20.3	144	120	>3	30	2D8	−1.03
MDM 22	05 23 41.01	−70 51 23.8	156	141	>3	30	2D8	−0.82
MDM 24	05 25 05.62	−68 37 00.7	8	8	>3	30	2D4	−0.23
MDM 25	05 25 17.22	−67 22 47.5	67	61	>3	30	2D1	+0.09
MDM 27	05 25 33.87	−68 41 20.9	6	6	>3	30	2D4	−0.92
MDM 28	05 26 11.92	−70 22 47.4	6	6	>3	30	2D7	−1.57
MDM 29	05 26 24.76	−68 15 14.6	14	14	>3	30	2D3	−1.16
MDM 30	05 26 35.34	−67 49 09.4	119	111	>0	30	2D2	+0.42
MDM 31	05 27 45.90	−67 59 27.1	39	46	>0	30	2D2	+0.41
MDM 32	05 27 49.20	−70 36 44.2	35	31	>3	30	2D8	−0.91
MDM 35	05 28 47.65	−68 36 22.9	22	24	>3	30	3D4	+0.24
MDM 38	05 29 51.64	−67 49 33.6	101	55	>3	30	3D2	−1.85
MDM 40	05 31 22.53	−70 11 54.5	5	6	>3	30	3D7	−1.24
MDM 42	05 31 43.93	−70 49 25.4	16	14	>3	30	3D8	−0.39
MDM 44	05 32 07.06	−67 54 14.3	22	18	>3	30	3D2	−1.15
MDM 45	05 32 09.69	−68 43 07.9	11	12	>3	30	3D4	+0.06
MDM 48	05 32 44.99	−70 01 28.7	48	47	>3	30	3D7	−0.78
MDM 50	05 32 50.28	−68 20 12.8	4	5	>3	30	3D3	−1.54
MDM 51	05 32 52.81	−69 46 22.8	22	18	>3	30	3D6	−0.95
MDM 52	05 32 53.18	−67 09 46.1	19	18	>3	30	3D1	−0.39
MDM 53	05 32 54.25	−70 40 28.3	25	25	>3	30	3D8	+0.95
MDM 55	05 33 18.55	−67 39 59.7	23	24	>3	30	3D2	−0.51
MDM 56	05 33 42.36	−68 46 04.0	18	9	>3	30	3D4	−2.33
MDM 60	05 35 26.68	−67 17 04.7	44	37	>2	30	4D1	−0.76
MDM 61	05 35 37.56	−68 55 08.2	72	64	>3	30	4D4	+0.11
MDM 62	05 36 05.04	−69 18 46.3	49	46	>3	30	4D5	−1.11
MDM 63	05 36 23.80	−70 25 43.6	9	10	>3	30	4D7	−0.26
MDM 64	05 36 36.41	−67 07 36.0	48	40	>2	30	4D1	−0.83
MDM 65	05 36 57.23	−69 13 29.0	116	110	>3	30	4D5	−0.56
MDM 66	05 37 36.88	−68 00 33.8	14	12	>3	30	4D3	−1.85
MDM 68	05 38 04.66	−69 53 37.2	29	33	>3	30	4D6	−1.17
MDM 70	05 38 16.32	−70 56 37.3	23	23	>3	30	4D8	+0.27
MDM 74	05 39 37.59	−69 45 27.6	61	51	>3	30	5D6	+0.38
MDM 75	05 39 45.85	−69 38 39.0	61	53	>3	30	5D6	+0.99
MDM 78	05 40 04.48	−69 44 38.9	15	18	>3	30	5D6	−0.32
MDM 79	05 40 10.42	−67 18 15.2	74	63	>3	30	5D1	−0.18
MDM 80	05 40 11.55	−69 19 54.9	26	19	>3	30	5D5	−1.11
MDM 82	05 41 27.21	−67 39 51.2	18	17	>3	30	5D2	−1.29
MDM 83	05 41 31.65	−70 46 27.9	11	13	>3	30	5D8	−0.70
MDM 84	05 41 33.09	−67 06 16.7	39	36	>3	30	5D1	−1.03
MDM 85	05 41 59.05	−68 15 43.1	27	28	>2	30	5D3	−0.21
MDM 86	05 42 44.56	−67 25 54.6	12	10	>3	30	5D1	−0.57
MDM 87	05 42 56.58	−70 17 34.7	4	4	>3	30	5D7	−1.85
MDM 89	05 43 14.53	−68 44 35.9	52	45	>3	30	5D4	−0.81
MDM 90	05 43 15.21	−68 06 53.7	76	43	>2	30	5D3	−1.71
MDM 91	05 43 17.02	−67 15 09.3	3	4	>3	30	5D1	−0.97
MDM 94	05 45 27.76	−69 46 22.5	10	7	>3	30	6D6	+0.04
MDM 95	05 45 50.27	−68 45 57.0	30	28	>3	30	6D4	−1.20
MDM 98	05 46 29.34	−70 26 44.3	30	30	>3	30	6D7	−0.95
MDM 100	05 47 45.35	−67 45 07.0	69	52	>2	30	6D2	−0.85
MDM 101	05 47 50.32	−67 28 03.2	12	9	>3	30	6D1	+0.96
MDM 102	05 47 51.27	−69 45 43.3	4	5	>3	30	6D6	−1.07
MDM 103	05 47 57.45	−70 20 16.2	7	7	>3	30	6D7	−1.01
MDM 105	05 48 55.24	−70 39 28.3	12	11	>3	30	6D8	−1.15
MDM 106	05 49 39.71	−69 38 23.9	10	10	>3	30	6D6	−0.62

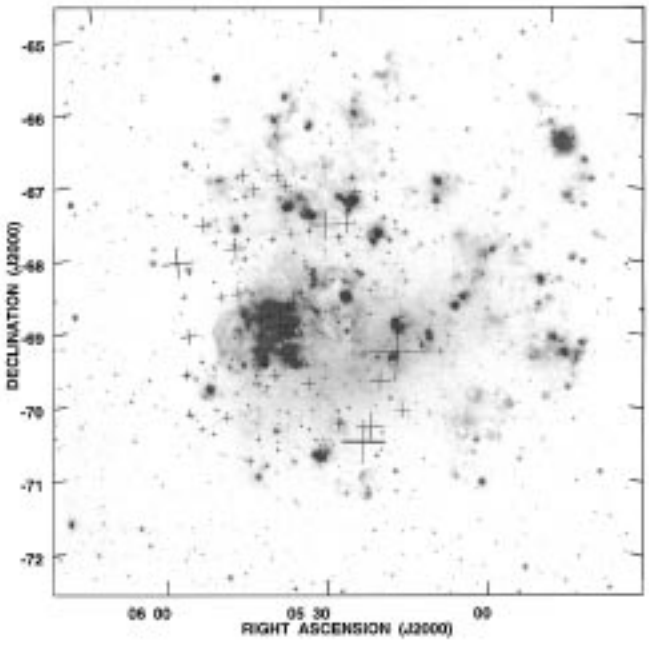

Fig. 3. Distribution of the compact radio sources on the Hα image of the LMC. The size of the crosses is proportional to the peak flux density of the source

high angular resolution performed with the aim at finding out which of the radio sources correspond to an optical emission knot, and which are background sources behind the DEM object, will be presented in a subsequent paper (Marx et al., in preparation).

5. Source counts

The ATCA source list of compact objects can be used to find the sky density of sources at 1.4 GHz in the direction of the LMC. Comparing the source counts with extragalactic source count results allows us to check for incompleteness of the snapshot survey and can be useful in determining the fraction of sources intrinsic to the LMC, which should appear as an excess of counts compared with the extragalactic ones. For this comparison the integrated flux density has to be used, since the peak flux depends on the telescope beam size. The differential source counts (number of sources with a given flux density) of the LMC snapshot survey have been calculated following the method described by Condon & Condon (1982) for their 1.411 GHz VLA snapshot survey.

The ATCA snapshot survey is complete above the uncorrected peak flux density limits given in Table 1. Corresponding limits to the primary beam corrected peak flux densities vary with location in each map, so that the solid angle Ω in which a source of given peak flux S_p can be detected increases with S_p. Each source counted must therefore be weighted by Ω^{-1} to give its proper contribution to the areal density of sources. For the calculation of $\Omega(S_\mathrm{p})$ the overlapping of the fields has been taken into account. The total counting area is 3.6 10^{-3} sr. The function $\Omega(S_\mathrm{p})$ is plotted in Fig. 4.

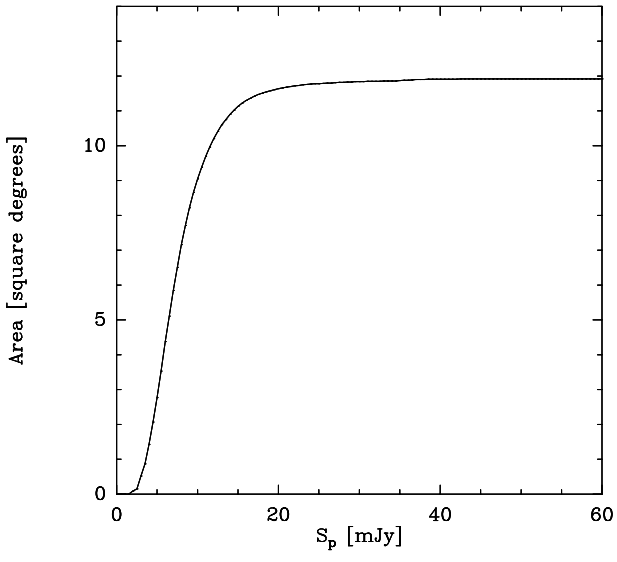

Fig. 4. Solid angle Ω in which a source with a given peak flux density has been counted

Since we want to find the sky number density of sources as a function of their integrated flux densities, we must allow for sources which are missing from the survey because they are extended. Such sources have peak flux densities, S_p, below the completeness limit and integrated flux densities, S_i, above this limit. We distinguish the continuum sources which are significantly resolved from those which are not by using the method of Willis et al. (1976). An observed source is defined as extended if

$$R \geq 1 + 2 \cdot \frac{2.47 \cdot \sigma}{S_\mathrm{p}}$$

R is the Gaussian fitted area divided by that of the antenna pattern ($R = \frac{\Theta_{S\max} \cdot \Theta_{S\min}}{\Theta_{B\max} \cdot \Theta_{B\min}}$) and σ is the rms noise in the area of the source after primary beam correction. Assuming that the angular-size distribution of sources as faint as 4 mJy is not significantly different from the angular-size distribution of sources in the range 35 mJy $\leq S_\mathrm{i} <$ 140 mJy (Downes et al. 1981), then the fraction of extended sources (0.27) in this flux density interval can be used to estimate the fraction of faint extended sources missing from the ATCA survey.

The source counts including all observed sources are listed in Table 5. The flux density interval (Col. 2) around S_c (Col. 1) is defined as $2^{-1/2} S_\mathrm{c} \leq S_\mathrm{i} < 2^{1/2} S_\mathrm{c}$. The number of resolved sources N_res and the number of unresolved sources N_unres found in each flux-density interval is shown in Cols. 3 and 4. The fraction of unresolved sources f_unres is listed in Col. 5. The mean fraction of unresolved sources

in the flux density range 35 mJy $\leq S_{\rm i} <$ 140 mJy is 0.27, so the correction factor K (Col. 6) is the fraction of unresolved sources in each flux density interval divided by 0.27. Column 7 shows the weighted, uncorrected number of sources per steradian

$$N_{\rm w} = \sum_{i=1}^{N} \frac{1}{\Omega(S_{p_i})}$$

with the 1 σ rms error (Garwood et al. 1988)

$$\Delta N_{\rm w} = \sqrt{\sum_{i=1}^{N} \frac{1}{\Omega^2(S_{p_i})}}.$$

The summation is taken over all sources in the flux density interval. The last column gives the corrected number of sources per flux density interval ($S_{\rm range}$) per steradian normalized to $n_0 = S_{\rm c}^{-2.5}$, meaning:

$$n \cdot S_{\rm c}^{2.5} = K \cdot \frac{N_{\rm w}}{S_{\rm range}} \cdot S_{\rm c}^{2.5}.$$

The source counts in the LMC snapshot fields are plotted in Fig. 5. The line in the figure represents the extragalactic source count distribution of the Westerbork survey at 1.4 GHz (Oosterbaan 1978). The differential source counts of this survey are well approximated by

$$n(S) = 311 \cdot S^{-2.59-0.106 \cdot \ln S} {\rm sr}^{-1} {\rm Jy}^{-1}.$$

The comparison of the ATCA snapshot survey to the Westerbork survey is difficult because the latter is sensitive to more extended structures compared to the ATCA survey. For extended sources we expect that the integrated flux densities of the snapshot sources are underestimated, which causes a higher uncertainty in the source count distribution; for more accurate integrated flux densities we would need more observations with shorter baselines. The LMC source count distribution, however, follows the extragalactic distribution of Oosterbaan very closely. This indicates that most of the compact sources of the LMC survey are background objects. At the highest flux density interval 280 mJy $\leq S_{\rm i} <$ 560 mJy there are two sources missing compared to the Westerbork survey. This might be due to the underestimated integral flux densities. An excess of sources above the extragalactic source counts is indicated in the flux density range from 8.8 to 35 mJy. The discrepency between the number of sources predicted and observed in the 8.8 to 35 mJy bin is only weakly significant, given the uncertainties in flux density in this survey. It suggests, that some of the fainter sources are associated with the LMC, a conclusion strongly supported by the positional coincidence with Halpha knots discussed above.

We get the best match to the extragalactic fit of Oosterbaan (see Fig. 5 lower panel and Table 5) by excluding all 15 possible intrinsic sources in the second and third flux density interval for which the position corresponds to a DEM object plus three known HII regions located in the N159 – N160 area (Marx et al., in preparation). So we conclude that only a few compact sources in directions toward the LMC are intrinsic objects, and that most of these have flux densities between 8.8 and 35 mJy and are located within extended Hα emitting regions.

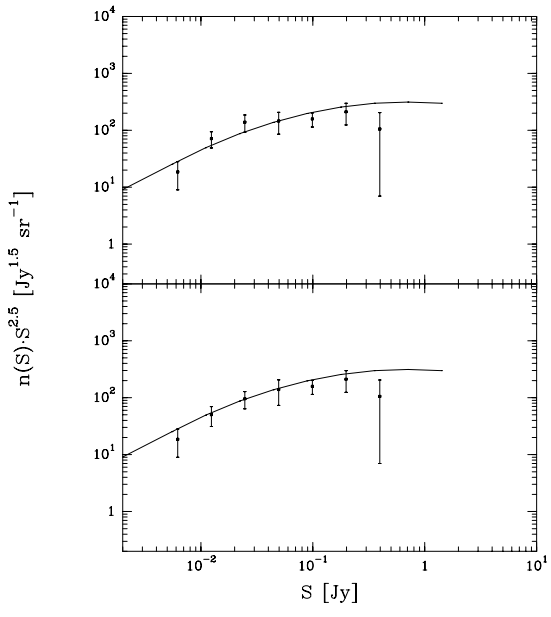

Fig. 5. Source counts for all sources of our survey (top). The line presents the source count distribution of Oosterbaan (1978). The lower panel shows the source counts after excluding all possible intrinsic sources and the known HII regions

6. Summary

A sample of 113 compact radio continuum sources has been detected in and behind the LMC at 1.4 GHz with the Australia Telescope Compact Array (ATCA); 70 objects have been found at 2.4 GHz. The sample is almost complete down to a flux density limit of about 6 mJy at 1.4 GHz for sources smaller than $D \sim 54''$ and about 3 mJy at 2.4 GHz for $D \sim 34''$ (see Table 1). As the sizes of the sources are smaller than 13 pc at 1.4 GHz and 8 pc at 2.4 GHz the objects are either extragalactic background sources or compact objects within the LMC, such as compact HII regions or young SNRs. The vast majority of our sources have been seen for the first time. This is due to the higher angular resolution of the ATCA compared to the instruments used for previous surveys.

Excluding the 15 sources which are located in the regions of Hα objects in the Davies et al. (1976) catalogue and which have flux densities in the 8.8 – 35 mJy range plus three known HII regions, we find that our source counts agree very well with those of Oosterbaan (1978). So we conclude that our catalogue of compact sources contains beyond the 3 known HII regions located in the

Table 5. Source counts

S_c [Jy]	flux density interval [Jy]	N_{res}	N_{unres}	f_{unres}	K	$10^{-3}N_w$ [sr^{-1}]	$n \cdot S^{2.5}$ [sr^{-1}Jy$^{1.5}$]
Source counts using all objects							
0.0062	$0.0044 \leq S_i < 0.0088$	0	12	1	3.7±1.5	7.3±2.3	18.6±9.6
0.0124	$0.0088 \leq S_i < 0.0175$	2	28	0.93	3.5±0.9	10.5±1.95	71.5±22.7
0.0247	$0.0175 \leq S_i < 0.0350$	3	24	0.89	3.3±0.9	7.7±1.5	139.2±46.8
0.0495	$0.0350 \leq S_i < 0.0700$	15	9	0.38	1.4±0.5	6.7±1.4	146.1±60.5
0.0990	$0.0700 \leq S_i < 0.1400$	11	2	0.15		3.6±1.0	158.6±44.1
0.1980	$0.1400 \leq S_i < 0.2800$	6	0	0		1.7±0.7	211.8±87.2
0.3960	$0.2800 \leq S_i < 0.5600$	1	0	0		0.3±0.28	105.7±98.7
Source counts excluding sources with 0.0088 Jy $\leq S_i <$ 0.035 Jy lying within DEM objects							
0.0062	$0.0044 \leq S_i < 0.0088$	0	12	1	3.7±1.5	7.3±2.3	18.6±9.6
0.0124	$0.0088 \leq S_i < 0.0175$	1	21	0.95	3.5±1.1	7.4±1.6	50.4±19.3
0.0247	$0.0175 \leq S_i < 0.0350$	2	16	0.89	3.3±0.8	5.3±1.2	95.8±31.9
0.0495	$0.0350 \leq S_i < 0.0700$	14	9	0.39	1.4±0.6	6.4±1.33	139.6±66.5
0.0990	$0.0700 \leq S_i < 0.1400$	11	2	0.15		3.6±1.0	158.6±44.1
0.1980	$0.1400 \leq S_i < 0.2800$	6	0	0		1.7±0.7	211.8±87.2
0.3960	$0.2800 \leq S_i < 0.5600$	1	0	0		0.3±0.28	105.7±98.7

N159 – N160 area only about 15 objects which are probably intrinsic to the LMC. More detailed observations of sources within the boundary of DEM objects will be presented in a subsequent paper.

Acknowledgements. We thank the staff of the ATCA for their assistance and advice. We are grateful for the hospitality of the ATCA at Narrabri and Epping during our visit. We thank the members of the Graduiertenkolleg in Bonn/Bochum for very useful discussions. Thanks are especially due to Uwe Herbstmeier for valuable suggestions and information. Jürgen Osterberg and Eva Grebel are thanked for providing us with data for comparisons. The research of M. Marx was supported by the Cusanuswerk (Bonn, Germany), U. Mebold was supported by the Deutsche Forschungsgemeinschaft under grant Me745/16-1. J. Dickey was supported in part by National Science Foundation grants 87-22990 and 92-22130 to the University of Minnesota, by a grant from the NSF Unique Foreign Telescope Fund supervised by the National Radio Astronomy Observatory, and by the Office of International Programs at the University of Minnesota.

References

Clarke J.N., Little A.G., Mills B.Y., 1976, Aust. J. Phys. Astrophys. Suppl. 40, 1
Clarke B., 1980, A&A 89, 355
Condon J.J., Condon M.A., 1982, AJ 87, 739
Davies R.D., Elliott K.H., Meaburn J., 1976, Mem. R. Astron. Soc. 81, 89
Dickey J.M., Mebold U., Marx M., Amy S., Haynes R.F., Wilson W., 1994, A&A 289, 357
Downes A.J.B., Longair M.S., Perryman M.A.C., 1981, MNRAS 197, 593
Filipovic M.D., Haynes R.F., White G.L., Jones P.A., Klein U., Wielebinski R., 1995, A&AS 111, 311
Garwood R.W., Perley R.A., Dickey J.M., Murray M.A., 1988, AJ 96, 1655
Habing H.J., Israel F.P., 1979, ARA&A 17, 345
Hunt M.R., Whiteoak J.B., 1994, Proc. Astron. Soc. Aust. 11, 68
Kennicutt R.C., Bresolin Jr., Bresolin F., Bomans D.J., Bothun G.D., Thompson I.B., 1995, AJ 109, 594
Lortet M.-C., Borde S., Ochsenbein F., 1994, A&AS 107, 193
McGee R.X., Brooks J.W., Batchelor R.A., 1972a, Aust. J. Phys. 25, 581
McGee R.X., Brooks J.W., Batchelor R.A., 1972b, Aust. J. Phys. 25, 613
Mills B.Y., Turtle A.J., 1984a, Proc. IAU Symp. 108, 283
Mills B.Y., Turtle A.J., Little A.G., Durdin M.J., 1984b, Aust. J. Phys. 37, 321
Oosterbaan C.E., 1978, A&A 69, 235
Westerlund B.E., Matthewson D.S., 1966, MNRAS 131, 371
Westerlund B.E., 1992, A&AR 2, 29
Willis A.G., Oosterbaan C.E., De Ruiter H.R., 1976, A&AS 25, 453
Wright A.E., Griffith M., Burke B., Ekers R.D., 1994, ApJS 91, 111